Universal Size-Dependent Trend in Auger Recombination in Direct-Gap and Indirect-Gap Semiconductor Nanocrystals

István Robel,[1] Ryan Gresback,[2] Uwe Kortshagen,[2] Richard D. Schaller,[1,*] and Victor I. Klimov[1,†]

[1]*Chemistry Division, Los Alamos National Laboratory, Los Alamos, New Mexico 87545, USA*

[2]*Department of Mechanical Engineering, University of Minnesota, Minneapolis, Minnesota 55455, USA*

(Received 19 December 2008; published 1 May 2009)

We report the first experimental observation of a striking convergence of Auger recombination rates in nanocrystals of both direct- (InAs, PbSe, CdSe) and indirect-gap (Ge) semiconductors, which is in contrast to a dramatic difference (by up to 4–5 orders of magnitude) in the Auger decay rates in respective bulk solids. To rationalize this finding, we invoke the effect of confinement-induced mixing between states with different translational momenta, which diminishes the impact of the bulk-semiconductor band structure on multiexciton interactions in nanocrystalline materials.

DOI: 10.1103/PhysRevLett.102.177404 PACS numbers: 78.67.Hc, 62.25.−g, 78.47.jc

Semiconductor nanocrystals (NCs) are nanometer-size crystalline particles that contain approximately 100–10 000 atoms. Strong spatial confinement of electronic excitations produced by these nanostructures results in a number of novel phenomena including greatly enhanced nonradiative Auger recombination (AR) [1–4]. In this process, the electron-hole recombination energy is not emitted as a photon but is transferred to a third particle (an electron or a hole). Significant interest in Auger effects in bulk and low-dimensional structures has been stimulated by studies of carrier-loss mechanisms in semiconductor lasers [5,6] and generation-III photovoltaics enabled by carrier multiplication [7–9] as well as Auger-assisted energy relaxation [3,10,11].

In bulk-phase semiconductors, AR rates differ significantly for direct- and indirect-gap materials. In direct-gap semiconductors, AR is a three-carrier process [Fig. 1(a)]. On the other hand, it is a lower-probability, four-particle effect in indirect-gap materials because of an additional step involving emission (or absorption) of a momentum-conserving phonon [Fig. 1(b)] [12]. Strong three-dimensional confinement obtained in NCs leads to relaxation of translational-momentum conservation, which might diminish the distinction between direct- and indirect-gap semiconductors with regard to AR [Fig. 1(c)]. Whereas the effect of quantum confinement on radiative recombination in indirect-gap materials has been considered in the literature [13–15], its influence on multiparticle processes has not been examined either theoretically or experimentally.

In this Letter, we report on a striking convergence of multiexciton behaviors in both direct- (InAs, PbSe, CdSe) and indirect-gap (Ge) semiconductors that results from quantum confinement. Specifically, our measurements indicate that similarly sized NCs of different compositions exhibit comparable AR rates despite a dramatic 4–5 orders of magnitude difference in respective bulk-semiconductor values. We further observe a universal, material-independent linear scaling of AR rates with NC volume (“V scaling”) indicating that the main factor which controls AR in NCs is particle dimension, while details of the material’s band structure play a minor role.

Since AR in NCs of direct-gap materials has been discussed in the literature [2,8,16,17], below we focus primarily on details of Ge NC experimental studies. In our work, we investigate Ge NCs fabricated via a plasma-based technique [18]. The mean NC radii R are from 1.9 to 5 nm, and the size dispersion is ~15%. To monitor carrier recombination dynamics, we employ a transient absorption (TA) spectroscopy in which photoinduced absorption associated with nonequilibrium carriers injected by a sub-100 fs, 1.55 eV pump pulse is probed with a second variably delayed pulse tuned to 1100 nm.

In Fig. 2(a), we display absorption spectra of Ge NCs of two sizes in comparison to that of bulk Ge [19]. While Ge NC spectra do not show any distinct band-edge features typical of direct-gap semiconductor NCs, the spectral onset of absorption shows a pronounced blueshift with respect to

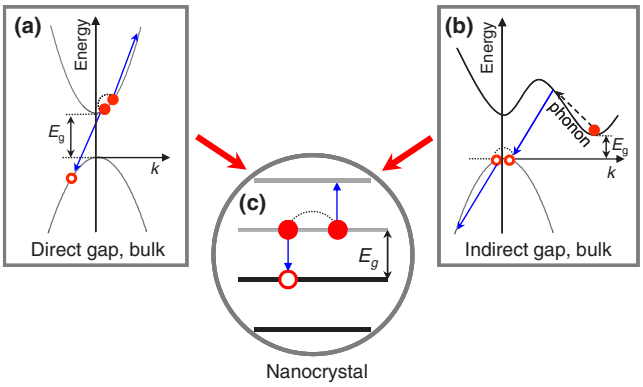

FIG. 1 (color online). (a) The three-particle AR process in direct-gap bulk semiconductors. (b) Phonon-assisted four-particle AR process in indirect-gap bulk semiconductors. (c) AR in NCs. Relaxation of momentum conservation requirements in NCs diminishes the difference between direct- and indirect-gap materials with regard to AR.

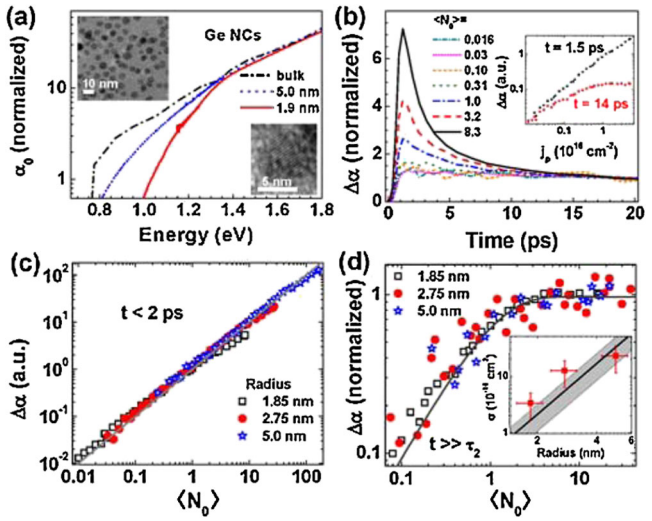

FIG. 2 (color online). (a) Linear absorption spectra of Ge NCs indicate an absorption onset, which is blueshifted in comparison to bulk Ge [19]. Insets: Examples of large-area (upper left corner) and high-resolution (lower right corner) transmission electron micrographs of Ge NCs indicating good size monodispersity and a high degree of crystallinity. (b) Pump-intensity-dependent TA dynamics of 1.85 nm radius Ge NCs for average initial exciton occupancies from 0.016 to 8.3. Inset: Pump-intensity dependence of early- and late-time TA signals. (c) Pump-intensity dependence of TA signals shortly after excitation for Ge NCs with radii of 1.85, 2.75, and 5.0 nm (symbols) fit to a linear dependence (line). (d) Long-time TA signals ($t \gg \tau_2$) as a function of $\langle N_0 \rangle$ fit to the Poissonian distribution describing the total number of photoexcited NCs. Inset: Absorption cross sections (symbols) derived from fits to experimental data in the main panel in comparison to calculations based on the R^3 scaling (line; the shaded region is the range of uncertainty due to the distribution in NC sizes).

bulk Ge, indicating a significant effect of quantum confinement.

In Fig. 2(b), we display TA dynamics recorded for a series of pump-photon fluences from $\sim 10^{14}$ to 5×10^{16} cm^{-2} that correspond to NC average initial occupancy $\langle N_0 \rangle = \langle N(t = 0) \rangle$ from 0.02 to 8 (estimated assuming an R^3 scaling of absorption cross sections [20] σ). The low-intensity TA traces ($\langle N_0 \rangle \leq 0.3$) are nearly flat, indicating that no significant carrier losses occur on the time scale of these measurements ($t \leq 20$ ps). As $\langle N_0 \rangle$ increases, a fast relaxation component of progressively larger amplitude develops in the TA signal. This behavior is typical of AR in the regime when multiple excitons are excited per NC [2].

A more conclusive assignment of the fast TA component is based on the analysis of pump-intensity dependences of TA signals. At short times after excitation ($t = 1$–2 ps), photoinduced absorption increases almost linearly with pump fluence across a wide range of $\langle N_0 \rangle$ from 0.01 to ~ 10 [inset, Fig. 2(b)]. A similar, nearly linear scaling is observed for all NC sizes studied here [Fig. 2(c)], indicating that the TA amplitude provides a quantitative measure of the average NC occupancy in both single- and multiexciton regimes.

Following AR, all initially excited NCs contain only single excitons independent of their initial occupancy. Therefore, the TA signal immediately following Auger decay represents a measure of the total number of photoexcited NCs. For short-pulse excitation well above the band edge, the distribution of N_0 in a NC ensemble is described by Poisson statistics [20]. In this case, the fraction of photoexcited NCs is represented by $[1 - \exp(\langle N_0 \rangle)]$, which accurately describes long-time TA signals [Fig. 2(d) and inset in Fig. 2(b)]. Further, using this expression as a fitting function, we derive experimental absorption cross sections and then compare them with calculations based on the R^3 scaling. Good agreement between the computed and the measured values of σ [inset in Fig. 2(d)] together with results of pump-intensity-dependent TA studies [Figs. 2(c) and 2(d)] support our assignment of the fast-decaying TA component to AR.

We isolate the biexcitonic component of the TA traces by subtracting the slowly varying single excitonic component measured at low intensities [2] ($\langle N_0 \rangle \ll 1$). We then derive biexciton lifetimes τ_2 either by directly fitting decays obtained for $\langle N_0 \rangle$ close to 1 or by analyzing the higher-intensity dynamics in the region where the average exciton multiplicity $\langle N_x \rangle$ (the average number of excitons per photoexcited NC) falls below 2. These lifetimes do not depend upon exact pump fluence [compare different types of symbols of the same color in Fig. 3(a)] but do exhibit a pronounced size dependence. Specifically, τ_2 varies from ~ 4 to ~ 100 ps for NCs with radii from 1.9 to 5 nm, approximately following the R^3 dependence [solid line in Fig. 3(b)]. This result, indicating linear scaling of τ_2 with NC volume, is similar to previous observations of V scaling for NCs of different compositions [2,21], which provides further evidence that the observed decay is indeed due to AR of multiexcitons.

In bulk semiconductors, the AR rate is characterized by the Auger constant C_A, which is defined assuming that the decay rate r_A is cubic in carrier density n: $r_A = dn/dt = -C_A n^3$. Strictly speaking, this definition may not always apply to NCs because, in this case, the r_A scaling can vary from quadratic ($r_A \propto N^2$) to cubic ($r_A \propto N^3$) or "statistical" [$r_A \propto N^2(N - 1)$], depending on the material-specific electronic structure, NC size, and shape [4]. While recognizing this issue, we still formally introduce the *effective* Auger constant for NCs, which we use as a tool for quantitative comparisons of AR efficiencies in NCs of different compositions and also between NCs and respective bulk solids.

Assuming cubic scaling of r_A with N and defining an effective carrier density as N/V_0 (V_0 is the NC volume), we obtain the following expression relating C_A to τ_2 [4]: $C_A = V_0^2(8\tau_2)^{-1}$. The C_A constants calculated for Ge NCs from the measured biexciton lifetimes are displayed in Fig. 3(c) in comparison to bulk Ge [22]. These data show

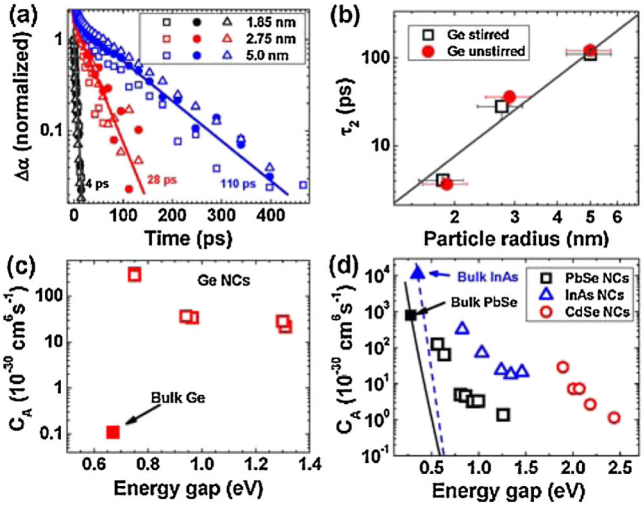

FIG. 3 (color online). (a) Biexcitonic decay component in Ge NCs as a function of NC size. Symbols are color-coded according to NC size, while different shapes correspond to different initial occupancies. (b) Biexciton lifetimes in Ge NCs (symbols) fit to the R^3 dependence (line). Stirred (squares) and unstirred (circles) samples produce essentially identical results, indicating that ionization and photodegradation processes do not affect our measurements. (c) Auger constants of bulk (solid square) and NC (open square) Ge as a function of E_g. (d) C_A in bulk (solid symbols) and NC (open symbols) forms of direct-gap semiconductors PbSe (squares), InAs (triangles), and CdSe (circles) as a function of E_g. Lines are projected values of C_A based on bulklike exponential dependences of Auger constants on E_g.

that C_A in Ge NCs, which varies from 2.1×10^{-29} to 2.8×10^{-28} $\mathrm{cm^6\,s^{-1}}$, is 2–3 orders of magnitude greater than the bulk Auger constant, indicating a significant confinement-induced enhancement in the AR efficiency.

To explain this enhancement, we invoke relaxation of translational-momentum conservation, which occurs as a result of confinement-induced spreading of electronic wave functions in k space [13]. In nominally indirect-gap materials, this effect can lead to significant mixing between electronic states from direct- and indirect-gap minima that can result in ''pseudodirect'' character of a band-edge transition [13–15]. A significant effect of spatial confinement on electronic structures of indirect-gap Si NCs has been experimentally detected using steady state [14] and time-resolved [15] photoluminescence as well as electron energy loss spectroscopy [23].

Our present results demonstrate that confinement-induced relaxation of crystal momentum also has a significant effect on the Auger process in indirect-gap semiconductors. In bulk Ge, the rate of Auger decay is greatly reduced in comparison to direct-gap semiconductors because of the participation of a momentum-conserving phonon [Fig. 1(b)]. Relaxation of momentum conservation in three-dimensionally confined NCs eliminates the phonon-assisted step in AR, which makes it a lower-order and, hence, a higher-probability process.

The breakdown of momentum conservation is also expected to affect AR in NCs of direct-gap materials. Because of combined requirements of energy and translational-momentum conservation, AR in direct-gap semiconductors exhibits a thermal-activation threshold (E_A) [12]. The relaxation of momentum conservation should remove this threshold and, hence, eliminate the strong exponential dependence of r_A on $-E_A/k_BT$ (k_B is the Boltzmann constant). This effect must dramatically change the dependence of Auger rates on the energy gap (E_g) since E_A is directly proportional to E_g. To analyze the effect of E_g on AR rates, we compare the values of C_A for NCs of different compositions.

From TA measurements conducted on PbSe and InAs NCs (not shown), we derive biexciton lifetimes and extract Auger constants. These data are displayed in Fig. 3(d) together with the C_A constants derived from literature data for CdSe NCs [2]. In the same plot, we also show values of C_A for bulk PbSe [24] and InAs [25]. We further use these values to calculate C_A for NCs of different E_g using the bulklike exponential dependence predicted by thermal-activation models [26,27]. The calculated values [shown by lines in Fig. 3(d)] exhibit much steeper decreases with increasing E_g than those derived from experiment (open squares and triangles). As a result, for each given E_g, the experimental C_A constant in NCs is orders of magnitude greater than the bulk-based projection. These observations are consistent with the expected elimination of the activation threshold.

While the energy gap is a key parameter of AR in bulk direct-gap semiconductors, it should be of lesser importance in the case of ''thresholdless'' AR in NCs. Indeed, as evident from Fig. 3(d), wide-gap CdSe NCs and narrow-gap PbSe NCs exhibit similar values of C_A, while AR rates in bulk forms of these materials are dramatically different [28]. Our present findings are also consistent with recent results of pressure-dependent studies of PbSe NCs [29], which have shown little effect of E_g (tuned by hydrostatic pressure) on AR rates.

Given the above considerations, an apparent change in NC Auger rates in Fig. 3(b) and Auger constants in Figs. 3(c) and 3(d) is *not* due to variations in E_g but rather due to changes in NC size. Therefore, one might expect the emergence of NC-specific trends in AR if C_A constants are analyzed as a function of NC radius instead of E_g. Such an analysis is presented in Fig. 4, where we plot C_A versus R for NCs of Ge, PbSe, InAs, and CdSe. Remarkably, despite a vast difference in electronic structures of the bulk solids (especially when one compares direct- and indirect-gap materials), the Auger constants in same-size NCs of different compositions are similar. Further, they show a universal cubic size dependence described approximately by $C_A = \gamma R^3$. The numerical prefactor in this expression (γ) varies by less than an order of magnitude (from 0.4×10^{-9} $\mathrm{cm^3\,s^{-1}}$ for CdSe NCs to 2.3×10^{-9} $\mathrm{cm^3\,s^{-1}}$ for Ge NCs) depending on composition,

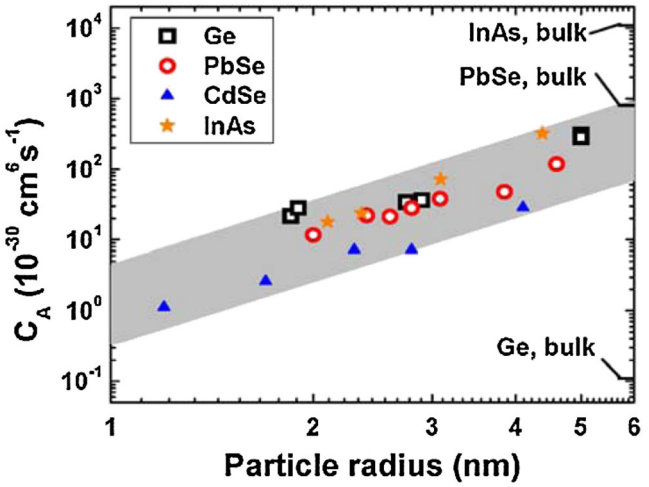

FIG. 4 (color online). Universal size dependence of AR constants in semiconductor NCs. When plotted as a function of NC radius, C_A values for NCs of both direct- and indirect-gap semiconductors show a similar size dependence described by $C_A = \gamma R^3$ (corresponds to the direction of the shaded stripe).

which is in sharp contrast to several orders of magnitude spread in Auger constants in the corresponding bulk materials (marked on the right axis of the graph in Fig. 4).

In spherical NCs, the effective Auger constant relates to the multiexciton decay rate constant ($K_N = \tau_N^{-1}$) as $C_A \propto R^6 K_N$ [4]. Therefore, the R^3 dependence of C_A suggests that K_N scales as R^{-3}, which is consistent with experimental results for Ge NCs in Fig. 3(b) as well as previous measurements of CdSe [2], InAs [16], and PbSe [8] NCs. The R^{-3} dependence indicates strong confinement-induced enhancement in Auger rates, pointing to multiple possible reasons. One is the size dependence of the strength of confinement-induced state mixing, which facilitates AR in NCs. This effect directly depends on the ratio of R^{-1} and Δk (separation of states in k space) and, hence, is enhanced with decreasing NC size [13–15]. Further, carrier-carrier Coulomb coupling, responsible for Auger decay, is expected to scale as $1/R$, which also contributes to enhanced Auger decay in smaller NCs. Finally, several existing models emphasize the importance of surface effects in AR in NCs [30,31], which may also result in increased rates of Auger decay with decreasing R because of increasing surface-to-volume ratio.

In summary, a close correspondence in Auger constants and multiexciton decay rates observed for similarly sized NCs of different compositions indicates that the key parameter, which defines Auger rates in these materials, is NC size rather than the energy gap or electronic structure details. These observations can be rationalized by confinement-induced relaxation of momentum conservation, which removes the activation barrier in Auger decay in NCs of direct-gap semiconductors and eliminates the need for a momentum-conserving phonon in indirect-gap NCs. Thus, this effect may diminish the difference between materials with different energy gaps (E_g would normally determine the height of the activation barrier) or different arrangements of energy bands in $\boldsymbol{k}$ space.

This work was supported by the Office of Basic Energy Sciences, U.S. Department of Energy (DOE) and Los Alamos LDRD funds and is part of the user program of the DOE Center for Integrated Nanotechnologies. R. G. and U. K. acknowledge partial support by the MRSEC Program of the National Science Foundation (DMR-0212302 and DMR-0819885).

*rdsx@lanl.gov
†klimov@lanl.gov

[1] D. I. Chepic *et al.*, J. Lumin. **47**, 113 (1990).
[2] V. I. Klimov *et al.*, Science **287**, 1011 (2000).
[3] L.-W. Wang *et al.*, Phys. Rev. Lett. **91**, 056404 (2003).
[4] V. I. Klimov *et al.*, Phys. Rev. B **77**, 195324 (2008).
[5] A. P. Mozer, S. Hausser, and M. H. Pilkuhn, IEEE J. Quantum Electron. **21**, 719 (1985).
[6] V. I. Klimov *et al.*, Science **290**, 314 (2000).
[7] T. P. Pearsall, Electron. Lett. **18**, 512 (1982).
[8] R. D. Schaller and V. I. Klimov, Phys. Rev. Lett. **92**, 186601 (2004).
[9] R. J. Ellingson *et al.*, Nano Lett. **5**, 865 (2005).
[10] Al. L. Efros, V. A. Kharchenko, and M. Rosen, Solid State Commun. **93**, 281 (1995).
[11] M. H. Pilkuhn, J. Lumin. **18/19**, 81 (1979).
[12] A. Haug, J. Phys. Chem. Solids **49**, 599 (1988).
[13] M. S. Hybertsen, Phys. Rev. Lett. **72**, 1514 (1994).
[14] D. Kovalev *et al.*, Phys. Rev. Lett. **81**, 2803 (1998).
[15] M. Sykora *et al.*, Phys. Rev. Lett. **100**, 067401 (2008).
[16] R. D. Schaller, J. M. Pietryga, and V. I. Klimov, Nano Lett. **7**, 3469 (2007).
[17] B. L. Wehrenberg, C. Wang, and P. Guyot-Sionnest, J. Phys. Chem. B **106**, 10 634 (2002).
[18] R. Gresback, Z. Holman, and U. Kortshagen, Appl. Phys. Lett. **91**, 093119 (2007).
[19] S. Adachi, J. Appl. Phys. **66**, 3224 (1989).
[20] V. I. Klimov, J. Phys. Chem. B **104**, 6112 (2000).
[21] M. C. Beard *et al.*, Nano Lett. **7**, 2506 (2007).
[22] D. H. Auston, C. V. Shank, and P. LeFur, Phys. Rev. Lett. **35**, 1022 (1975).
[23] P. E. Batson and J. R. Heath, Phys. Rev. Lett. **71**, 911 (1993).
[24] R. Klann *et al.*, J. Appl. Phys. **77**, 277 (1995).
[25] K. L. Vodopyanov *et al.*, Phys. Rev. B **46**, 13 194 (1992).
[26] P. R. Emtage, J. Appl. Phys. **47**, 2565 (1976).
[27] A. R. Beattie and P. T. Landsberg, Proc. R. Soc. A **249**, 16 (1959).
[28] Whereas Auger decay is fairly efficient in narrow-gap PbSe bulk crystals [24], it is not clearly resolvable in wide-gap CdSe, where radiative processes dominate [therefore, in Fig. 3(d) we do not show C_A for bulk CdSe].
[29] J. M. Pietryga *et al.*, Phys. Rev. Lett. **101**, 217401 (2008).
[30] A. L. Efros, D. J. Lockwood, and L. Tsybeskov, *Semiconductor Nanocrystals: From Basic Principles to Applications* (Kluwer, New York, 2003).
[31] A. Pandey and P. Guyot-Sionnest, J. Chem. Phys. **127**, 111104 (2007).